IJE TRANSACTIONS A: Basics Vol. 30, No. 4, (April 2017) 567-574

International Journal of Engineering

Journal Homepage: www.ije.ir

Robust Attitude Control of Spacecraft Simulator with External Disturbances

M. Malekzadeh*, B. Shahbazi

Department of Mechanical Engineering, University of Isfahan, Iran

PAPER INFO

Paper history:
Received 18 April 2016
Received in revised form 04 January 2017
Accepted 14 February 2017

Keywords:
Spacecraft Attitude Control Simulator
Linear Matrix Inequality
Robust Adaptive Controller
Hardware in the Loop

ABSTRACT

The spacecraft simulator robust control through H_∞-based linear matrix inequality (LMI) and robust adaptive method is implemented. The spacecraft attitude control subsystem simulator consists of a platform, an air-bearing and a set of four reaction wheels. This set up provides a free real-time three degree of freedom rotation. Spacecraft simulators are applied in upgrading and checking the control algorithms' performance in the real space conditions. The LMI controller is designed, through linearized model. The robust adaptive controller is designed based on nonlinear dynamics in order to overcome a broader range of model uncertainties. The stability of robust adaptive controller is analysed through Lyapunov theorem. Based on these two methods, a series of the laboratory and computer simulation are made. The tests' results indicate the accuracy and validity of these designed controllers in the experimental tests. It is observed that, these controllers match the computer simulation results. The spacecraft attitude is converged in a limited time. The laboratory test results indicate the controller ability in composed uncertainty conditions (existence of disturbances, uncertainty and sensor noise).

***doi**: 10.5829/idosi.ije.2017.30.04a.15*

1. INTRODUCTION

There exist several methods in checking the spacecraft attitude control subsystem performance. To verify controller algorithm in practical conditions, experimental tests are of essence [1]. The spacecraft simulator can create a real space environment in a limited laboratory on the ground for testing the designed controllers [2]. The experimental tests are more realistic, even with the effect of the gravity and high friction influences in comparison with the computer simulations. Recent advances in the design of such simulation platforms have made available more degrees of freedom, permitting greater movability which in turn, allowed the accomplishment of modern missions e.g., formation flying [3], rendezvous and docking [4, 5] in laboratory situ.

Model-based methods need that reliable equations of motion be derived in the hope that hidden dynamics such as flexibility effects or frictions could be avoided or evaluated within a bounded measure of uncertainty. In order to estimate the inertia and mass distribution of the simulator, a recursive least-square approach is proposed [6]. The reaction wheels friction is obtained by adopting methods in reference [7].

To examine the practical implementation of different control algorithms, the spacecraft attitude control subsystem are applied in references [8, 9]. An SDRE controller is applied to a 3-DOF SACS to test formation-flying maneuvers [10]. In literature [11], a 3D Cube Sat simulator is used to validate a quaternion feedback controller in realistic conditions.

In reference [12], The μ-synthesis control technique is applied in designing robust control laws for a satellite made of rigid and flexible panels. The μ-synthesis and super twisting sliding mode controllers are applied on a three degree of freedom satellite simulator in the reference [13]. A survey of the high performance robust attitude control is presented by Mazinan [14]. By linearization plant and producing an LTI state-space model of the system, a linear matrix inequality (LMI) control method can be designed as a specific robust controller. The LMI and adaptive methods are applied in literatures [15, 16] for controlling a non-linear system. Because of uncertainty in spacecraft features, applying robust controllers are necessary.

*Corresponding Author's Email: m.malekzadeh@eng.ui.ac.ir (M. Malekzadeh)

In this article, the performance of robust adaptive and LMI controllers are assessed. These robust strategies compensate the composite uncertain conditions.

The H_∞-based LMI controller is robust against a whole range of uncertainties and disturbances [17]. The robust adaptive controller is designed through Lyapunov theory and Barbalat's lemma [18]. The robust adaptive method is designed through nonlinear dynamics, the stability of which is proved. The performance of this method is compared with the available designed controllers in the presence of composed uncertainties (sensor noises, environmental disturbances and parametric uncertainties).

These newly developed controllers are applied in spacecraft attitude control subsystem simulator as the hardware in the loop.

The LMI linear controller and the nonlinear robust adaptive controller are applied in spacecraft simulator in the presence of uncertainty. The performance and robustness of both methods are assessed through several simulations.

The remainder of this article develops as follows**:** the simulator dynamics and linearized model are described in Section 2; the controller is designed in Section 3; the spacecraft simulator attitude control subsystem is designed in Section 4; the simulations are presented in Section 5 and the study concluded in Section 6.

2. SIMULATOR MODELLING AND DYNAMICS

2. 1. Dynamic Equations of Spacecraft Simulator

The Spacecraft attitude control subsystem simulator is illustrated in Figure 1. This simulator consists of three components: a holder, an air-bearing for creating weightlessness in real space conditions and a platform. The attitude dynamic equations of this simulator in quaternion form (in the inertia coordinate frame) can be expressed as [19]:

$$\dot{q}_i = \frac{1}{2}B(\vec{\omega})q \,,\quad J\dot{\omega}_i = -\omega_i \times J\omega_i + \tau_i \tag{1}$$

where, τ_i, J, ω_i and q are the control torque, spacecraft inertia matrix, the spacecraft angular velocity and quaternion vectors, respectively. The quaternion q is represented as: $q^T = [\vec{q} \;\; q_4]$; where, $\vec{q}$ is a 3×1 vector and q4 is a scalar.

The matrix B here is defined as:

$$B(\vec{\omega}) = \begin{bmatrix} 0 & \omega_z & -\omega_y & \omega_x \\ -\omega_z & 0 & \omega_x & \omega_y \\ \omega_y & -\omega_x & 0 & \omega_z \\ -\omega_x & -\omega_y & -\omega_z & 0 \end{bmatrix} \tag{2}$$

where,

$$\vec{\omega} = \left[\omega_x, \omega_y, \omega_z\right]^T \tag{3}$$

2. 2. Linearized Dynamic Equation of the Simulator

For small variation in the attitude states, the quaternion vectors with respect to the reference coordinate are obtained as [20]:

$${}^{s}_{R}q \approx \begin{bmatrix} \delta q_1 \\ \delta q_2 \\ \delta q_3 \\ 1 \end{bmatrix} \equiv \begin{bmatrix} \delta q \\ 1 \end{bmatrix} \tag{4}$$

where, ${}^{s}_{R}q$ is the spacecraft quaternion with respect to the reference frame. By inserting Equation (4) in Equation (1) and applying a first-order Taylor series, the linearized equations is expressed as:

$$\frac{d}{dt}\begin{bmatrix} \delta\vec{\omega} \\ \delta q \end{bmatrix} = A\begin{bmatrix} \delta\vec{\omega} \\ \delta q \end{bmatrix} + B\vec{U} \tag{5}$$

where,

$$A = \begin{bmatrix} 0 & 0 & 0 & -6\omega_0\sigma_x & 0 & 0 \\ 0 & 0 & \omega_0\sigma_y & 0 & 6\omega_0\sigma_y & 0 \\ 0 & \omega_0\sigma_z & 0 & 0 & 0 & 0 \\ 0.5 & 0 & 0 & 0 & 0 & 0 \\ 0 & 0.5 & 0 & 0 & 0 & \omega_0 \\ 0 & 0 & 0.5 & 0 & -\omega_0 & 0 \end{bmatrix}$$

$$\sigma_x = \frac{J_y - J_z}{J_x}, \sigma_y = \frac{J_z - J_x}{J_y}, \sigma_z = \frac{J_x - J_y}{J_z} \tag{6}$$

$$\vec{U} = \begin{bmatrix} \tau_x \\ \tau_y \\ \tau_z \end{bmatrix}, B = \begin{bmatrix} I^{-1} \\ O_{3\times 3} \end{bmatrix} = \begin{bmatrix} \frac{1}{J_x} & 0 & 0 \\ 0 & \frac{1}{J_y} & 0 \\ 0 & 0 & \frac{1}{J_z} \\ 0 & 0 & 0 \\ 0 & 0 & 0 \\ 0 & 0 & 0 \end{bmatrix}$$

Figure 1. Satellite simulator

and ω_0 is the circular orbital angular velocity of the spacecraft, which is zero in this equation. The parameters U, Jx, Jy and Jz are the input control and the diagonal terms of inertia matrix, respectively.

3. CONTROLLER DESIGN

3. 1. LMI Controller Synthesis An H_∞-based LMI controller is designed according to Guglieri et al. [17]. To design an H_∞-based LMI controller; the linear time invariant system dynamics are expressed in the following state space form:

$$\dot{x}(t) = Ax(t) + Bu(t) + d(t) \tag{7}$$

where, d is the external disturbance vector. Among the two theorems, the number one below is applied to design an H_∞-based LMI controller.

Theorem 1: For the uncertain spacecraft system Equation (7), by considering parametric uncertainties in the inertia matrix, applying the control feedback $u=Kx$ with a constant gain K, the following equation is yieled:

$$A = A_0 + (B + \Delta B)K \tag{8}$$

where, A_0 is the nominal plant. The inertia uncertainty is the most important parameter. By substituting J with $J_0+\Delta J$ in the B matrix (6), the following is yield:

$$B_i + \Delta B_i = \frac{1}{J+\Delta J} = \frac{1}{J(1+\frac{\Delta J}{J})} = \frac{1}{J}(1-\frac{\Delta J}{J}), \quad \Delta B_i = -\frac{\Delta J_{ii}}{J_{ii}^2} \tag{9}$$

According to reference [17] for the uncertain system, Equation (9), and given scalar $\gamma>0$, by appling controller gain, Equation (13), the closed loop system is asymptotically stable in a robust manner and $\left\| \frac{E(s)}{d(s)} \right\|_\infty < \gamma$ is guaranteed, provided that scalars $\rho>0$, α_i $(i=1,2,4)$ and $\beta_i>0$ $(i=1,2)$, and matrices S, L, $\tilde{P}_1>0$ hold true, where,

$$\begin{bmatrix} E_{11} & E_{12} & \alpha_2 d & S^T C^T & \alpha_1 S^T & \alpha_2 S^T \\ E_{12} & E_{22} & \alpha_1 d & 0 & 0 & 0 \\ \alpha_2 d & \alpha_1 d & -\gamma I & 0 & 0 & 0 \\ S^T C^T & 0 & 0 & -\gamma I & 0 & 0 \\ \alpha_1 S^T & 0 & 0 & 0 & -\beta_1 I & 0 \\ \alpha_2 S^T & 0 & 0 & 0 & 0 & -\beta_2 I \end{bmatrix} < 0 \tag{10}$$

and the actuator saturation condition is presented as follows:

$$\begin{bmatrix} u\,I & L \\ L & \frac{1}{\rho}\tilde{P} \end{bmatrix} \geq 0, \quad \begin{bmatrix} \rho & \alpha_4 q(0)^T \\ \alpha_4 q(0)^T & \alpha_4 S + \alpha_4 S^T - \tilde{P}_1 \end{bmatrix} \geq 0 \tag{11}$$

where,

$$\begin{aligned} E_{11} &= \alpha_2 S^T A^T + \alpha_2 AS + \alpha_2 BL + \alpha_2 L^T B^T + \beta_2 \alpha^2 I \\ E_{12} &= P_1 - \alpha_2 S + \alpha_1 S^T A^T + \alpha_1 L^T B^T \\ E_{22} &= -\alpha_1 S - \alpha_1 S^T + \beta_1 \alpha^2 I \end{aligned} \tag{12}$$

and:

$$K = LS^{-1} \tag{13}$$

Proof: The proof is in reference [17].

3. 2. Robust Adaptive Controller Synthesis The attitude equation of the formation with a limited disturbance $\dot{\omega} = J^{-1}(-\omega \times J\omega) + J^{-1}u + d$ can be written in the following affine form:

$$\dot{\omega} = F(\omega) + Gu + d \quad F \in R^n, \tag{14}$$

where,

$$F(\omega) = J^{-1}(-\omega \times J\omega) \qquad G = J^{-1} \tag{15}$$

considering uncertainty ΔJ in the inertia moment yields

$$F(\omega) = (J+\Delta J)^{-1}(-\omega \times (J+\Delta J)\omega) \tag{16}$$

By assumption $|\Delta J/J|<1$, applying Binomial series, we can write:

$$\begin{aligned} (J+\Delta J)^{-1} &= \frac{1}{J(1+\frac{\Delta J}{J})} = J^{-1}(1-\frac{\Delta J}{J}+\ldots) \\ &= J^{-1}(1-\frac{\Delta J}{J}) = J^{-1} - J^{-2}\Delta J \end{aligned} \tag{17}$$

By ignoring ΔJ with respect to J in $(J+\Delta J)$, one obtains

$$F(\omega) = J^{-1}(-\omega \times J\omega) + J^{-2}\Delta J(\omega \times J\omega) \tag{18}$$

By defining:

$$F(\omega) = N(\omega) + \Delta F(\omega) \tag{19}$$

where, $N(\omega)$ is the known part of $F(\omega)$ and $\Delta F(\omega)$ is its unknown term.

$$N(\omega) = J^{-1}(-\omega \times J\omega), \quad \Delta F(\omega) = J^{-2}\Delta J(\omega \times J\omega) \tag{20}$$

Concerning with the inertia changes, caused by the fuel consumption, time-varying parametric uncertainties may be also incorporated in $F(\omega)$ as:

$$F(\omega) = N(\omega) + \Delta F(\omega) + \sigma(\omega)T(t), \tag{21}$$

In which, $T(t)$ denotes a time-varying parameter vector and $\sigma(\omega)$ is a state dependent regressor. In this paper, this term is ignorable. If the thruster are applied as actuator, this term play an important role.

The model uncertainty in G matrix, $\Delta G.u$ is considered in unknown and time varying terms. as:

$$\Delta F(\omega) \leq L(\omega), \quad T(t) \leq a \quad a>0 \tag{22}$$

where, a is an unknown constant parameter; while $L(\omega)$ is a state function (not a specified constant) which make this approach a generality in designing. *G* must be a positive definite matrix and assume that *r* is the lower bound of:

$$G \geq r.I \tag{23}$$

If the error is introduced as $E=\omega_i-\omega_i^d$, the error dynamic can be expressed as follows:

$$\dot{E}=N(\omega)+\Delta F(\omega)+\sigma(\omega)T(t)+G.u+d\text{-}\dot{\omega}^d \tag{24}$$

The Controller is developed through:

$$\begin{aligned} u &= -\frac{1}{r}\left[u_r+u_a+KE+\frac{H^2(\omega)E}{H(\omega)E}\right]-K_q\Lambda^T\vec{q}_e \\ \Lambda &= \frac{1}{2}\left[q_{e4}I+(\vec{q}_e)^{\times}\right] \end{aligned} \tag{25}$$

where, $K_q=G^{-1}$ and $K^T=K$ is a symmetric matrix. The quaternion error is defined as:

$$q_e=q_d-q=\begin{bmatrix}\vec{q}_e\\ q_{4e}\end{bmatrix} \tag{26}$$

The robust adaptive controller is composed of u_a, adaptive controller and u_r, robust controller and $K_q\Lambda^T\vec{q}_e$ is added in order to expose the desired quaternion effect (or quaternion error $\vec{q}_e$). The function $H(\omega)$ is defined as:

$$H(\omega)=L(\omega)+N(\omega)+\dot{\omega}^d \tag{27}$$

Theorem 2: If the controlling terms and controller gains are defined as follows, the system will be asymptotically stable.

$$u_r=\frac{E}{2\beta},\quad u_a=\hat{a}\frac{\sigma(\omega)\sigma(\omega)^T E}{\sigma(\omega)^T E} \tag{28}$$

where,

$$\dot{\hat{a}}=\rho_a\sigma(\omega)^T E,\ \hat{a}(0)>0 \tag{29}$$

and ρ_a is the adapt coefficient:

$$\beta,\ \rho_a>0 \tag{30}$$

Proof: The Lyapunov function is considered in this case as follows:

$$V(E,\hat{a},\vec{q}_e)=\frac{1}{2}E^TE+\frac{1}{2\rho_a}\tilde{a}^2+\frac{1}{2}\vec{q}_e{}^T\vec{q}_e \tag{31}$$

By defining:

$$\tilde{a}=a-\hat{a}, \tag{32}$$

where, $\hat{a}$ is an estimate of *a* and by taking derivative of (32), $\dot{\tilde{a}}=-\dot{\hat{a}}$ is yielded. The derivation of previous Lyapunov function is as follows:

$$\begin{aligned} &\dot{V}(E,\hat{a},\vec{q}_e)=\left(N(\omega)+\Delta F(\omega)+\sigma(\omega)T(t)\right)^T E \\ &+d^TE+\dot{\omega}^{dT}E \\ &+u^TG^TE+\frac{1}{\rho_a}\tilde{a}\dot{\tilde{a}}+\vec{q}_e{}^T\dot{\vec{q}}_e \\ &\dot{\vec{q}}_e=\Lambda E,\ K^T=K \end{aligned} \tag{33}$$

By inserting H(ω) into Equation (24), the control effort and by applying $G\geq r.I$ the following inequality is obtained:

$$\begin{aligned} &\dot{V}(E,\hat{a},\vec{q}_e)\leq -E^TKE+N^T(\omega)E+\Delta F^TE \\ &+T(t)^T\sigma(\omega)^TE+\dot{\omega}^{dT}E-\frac{E^TH^2(\omega)E}{H(\omega)E} \\ &-\frac{1}{r}u_r^TG^TE+d^TE-\frac{1}{r}u_a^TG^TE-\frac{1}{\rho_a}\tilde{a}\dot{\hat{a}} \\ &-\vec{q}_e{}^T\Lambda(G^{-1})^TG^TE+\vec{q}_e{}^T\Lambda E \end{aligned} \tag{34}$$

Hence, it is worth mentioning that Equation (35) holds true:

$$\begin{aligned} &-\frac{1}{r}u_r^TG^TE+d^TE\leq -\frac{1}{2\beta}E^TE-\frac{1}{2}\beta d^Td+d^TE+\frac{1}{2}\beta d^Td \\ &=-\frac{1}{2\beta}\left(E^TE+\beta^2d^Td-2E^T\beta d\right)+\frac{1}{2}\beta d^2 \end{aligned} \tag{35}$$

By applying Equation (27) and by replacing $-\frac{1}{r}u_r^TG^TE+d^TE$ with its upper bound, the Equation (34) can be rewritten as:

$$\begin{aligned} &\dot{V}(E,\hat{a},\vec{q}_e)\leq -E^TKE+H(\omega)E-H(\omega)E \\ &-\frac{1}{2\beta}(E-\beta d)^T(E-\beta d)+\frac{1}{2}\beta d^2 \\ &+a\sigma(\omega)^TE-\hat{a}\sigma(\omega)^TE-\frac{1}{\rho_a}\tilde{a}\dot{\hat{a}} \end{aligned} \tag{36}$$

It is clear that the term $\frac{1}{2\beta}(E-\beta d)^T(E-\beta d)$ can be eliminated from the right side of Equation (36) and by replacing $\dot{\hat{a}}$, Equation (37) is yielded:

$$\dot{V}(E,\hat{a},\vec{q}_e)\leq -E^TKE+\frac{1}{2}\beta d^2 \tag{37}$$

By defining an integral from both sides of inequality in $\forall 0\leq\tau<\infty$:

$$\begin{aligned} &\int_0^\tau E^TKEdt+V\left(E(\tau),\tilde{a}(\tau)\right)\leq V\left(E(0),\tilde{a}(0)\right) \\ &+\frac{1}{2}\beta\int_0^\tau d^2dt \qquad \forall 0\leq\tau<\infty \end{aligned} \tag{38}$$

It is observed that here error norm is bounded. By using Barbalat's Lemma [18] and assuming $\|d\| \le D, D > 0$:

$$\dot{V} \le -\delta_k E^2 + \frac{1}{2}\beta D^2 \tag{39}$$

If $\delta_k > \frac{\beta D^2}{2\varepsilon}$, where, ε is any small $\varepsilon > 0$, we have:

$$\begin{aligned} &\dot{V} \le -\Delta E^2 < 0 \\ &0 < \Delta \end{aligned} \tag{40}$$

A positive $\Delta>0$ would prove the theorem.

4. SPACECRAFT SIMULATOR ATTITUDE CONTROL SUBSYSTEM

By applying the above mentioned robust controllers, the system is capable of compensating disturbances and uncertainties. To begin with, the efficiency of these proposed controllers are computer simulated.

The spacecraft attitude control subsystem simulator is generally composed of the following components:

- An in situ computer, to implement designed controller
- A motor driver
- Four reaction wheels as actuators, applying torque to the platform
- The AHRS sensor, to measure the attitude and angular velocity

A PC is connected to the simulator computer using Wi-Fi, which makes the system monitoring possible.

The spacecraft simulator platform mass and inertia moment are *m*=40 (kg) and

$$J = \begin{bmatrix} 1.8 & 0.12 & -0.02 \\ 0.12 & 1.7 & -0.02 \\ -0.02 & -0.02 & 3.4 \end{bmatrix}$$ (kg-m^2)

The general 3-D simulator model is illustrated in Figure 1. As observed, it has a disk-shaped platform, supported on a plane with a spherical air bearing. The related equipment like sensors, actuators, computer and its respective interface and electronic devices are attached to the platform. The simulator dynamic equation is expressed as:

$$\begin{aligned} &\dot{\omega}_i = J_i^{-1}\left(-\omega_i \times J_i\omega_i\right) + J_i^{-1}u + d \\ &+[-mgr_z\phi, -mgr_z\theta, 0] \end{aligned} \tag{41}$$

where, $[-mgr_z\phi, -mgr_z\theta, 0]$ is the disturbance caused by the difference between the center of mass and geometric center of the platform. The terms in Equation (41) were previously considered in the controller design.

The reaction wheel actuator torque generated from the dynamic and friction modeling is defined as:

$$\begin{aligned} &T_f = \begin{cases} T_s + b_w\omega_w & \omega_w \ne 0 \\ T_{s0} & \omega_w = 0 \quad \text{and} \quad \|T_m\| > \|T_{s0}\| \\ T_m & \omega_w = 0 \quad \text{and} \quad \|T_m\| < \|T_{s0}\| \end{cases} \\ &T_s = T_{s0}\sin(\omega_w) \\ &\dot{h}_\omega = T_m - T_f \end{aligned} \tag{42}$$

where, T_f, T_{s0}, T_m, b_w and ω_w are the frictional torque, Coulomb friction torque, mechanical torque to the Reaction wheel, viscous friction coefficient and the angular velocity of reaction wheels, respectively.

According to the practical tests carried out on the hardware, the minimum current required to drive the motors is 70 mA, hence, $T_{s0} = 70 * 0.0000441 = 0.003$. The motor viscous friction coefficient is considered as $b_w = 5.2*10^{-6}$.

Input constraint and angular momentum of reaction wheels are modeled as follows:

$$\begin{aligned} &T_{out} = \begin{cases} T_{in} & T_{in} \le T_{\max motor} \\ 0 & h_{\max} \ge h_{\max motor} \\ T_{\max motor} & T_{in} \ge T_{\max motor} \end{cases} \\ &h_{out} = \begin{cases} \int T_{in} & \int T_{in} \le h_{\max motor} \\ h_{\max motor} & \int T_{in} \ge h_{\max motor} \end{cases} \end{aligned} \tag{43}$$

where, T_{in}, T_{out}, $T_{\max motor}$, h_{out} and $h_{\max motor}$ are the calculated Torque of The controller, the torque command to the motor, maximum motor torque, motor output and maximum angular momentum.

Euler angles output of the sensor along the x and z-axis are ± 180 ° and the y-axis is ± 90 °. For more realistic results, the sensor noises in measuring angles and angular velocity are applied in simulations, in accordance with the sensor technical specifications catalogue. A White noise is added to Euler angle outputs, which is presented as $PSD(rad^2/Hz) = \text{noise power} = \sigma^2 B_w$.

where, σ^2 is the standard deviation. B_w is the bandwidth of the sensor in hertz. According to the sensor catalogue, the White noise specification is σ=0.5, Bw= 400 Hz, PSD=1.9*10^{-7} rad^2Hz and sample time is $123(Hz)\sec$. Based on the measurements taken during implementation,the accuracy of attitude sensor is 0.5 °. The power of the angular velocity sensor based on sensor catalogues is expressed as: PSD=3.23*10^{-7}rad^2Hz. The sensor static and dynamic accuracies are 0.5 °and 2°, respectively. The aerodynamic disturbances are modeled as follows:

$$d = [0.1, 0.1, 0.01].\left(\omega^2\right).sign(\omega) \tag{44}$$

Another disturbance torque here is the air bearing disturbance. The bearing errors due to manufacturing appear as a constant torque around the z-axis. This torque is calculated as $8.1 * 10^{-6}$ N.m by the test results.

5. SIMULATION

The computer simulations and hardware tests are made and ran with initial value of $[\varphi,\theta,\psi]$ =(-5,-15,100) in uncertain condition. The simulator attitude, angular velocity and control effort of the robust adaptive and LMI controllers are illustrated in Figures (2 and 4), (3 and 5) and (6 and 7), respectively.

As observed, the two controllers perform well in composite uncertain conditions. Comparing Figures (2,4), the Euler angles can converge in smaller settling time, in LMI method. The LMI method outperforms the adaptive method.

By comparing Figures 6 and 7, it is found that the maximum control effort is smaller in adaptive method.

In small duration maneuvers, simulator responses are similar to that achieved by computer simulations with a slight difference probably caused by damping terms not reflected in the dynamics equation of the simulator.

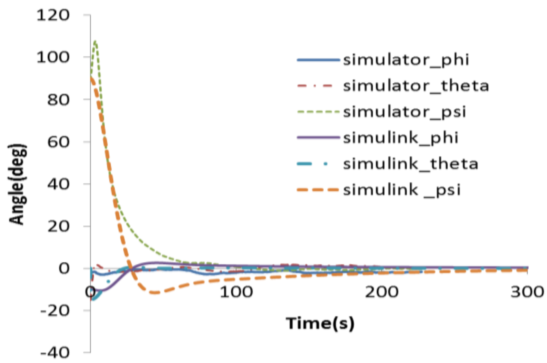

Figure 2. Comparison of the present numerical results with the experimental data of angles for Robust adaptive method

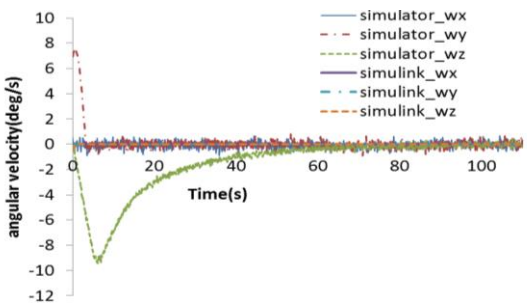

Figure 3. Comparison of the present numerical results with the experimental data of angular velocity for Robust adaptive method

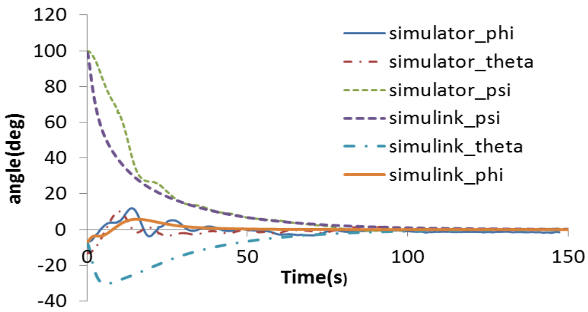

Figure 4. Comparison of the present numerical results with the experimental data of angles for LMI method

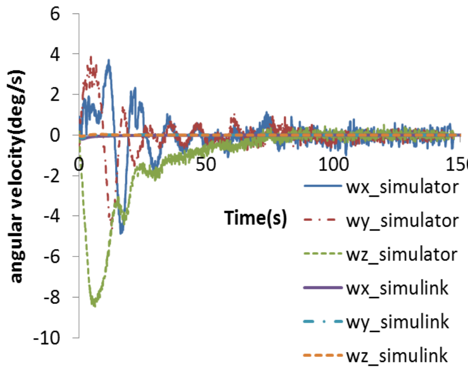

Figure 5. Comparison of the present numerical results with the experimental data of angular velocity for LMI method

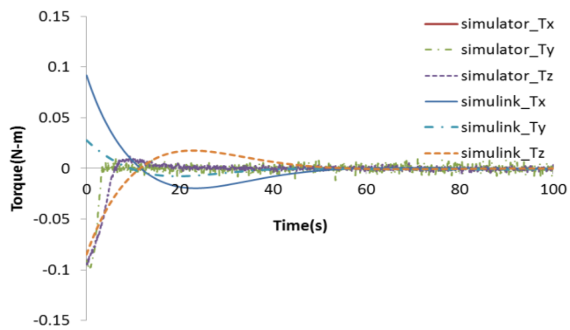

Figure 6. Control effort in Robust adaptive method

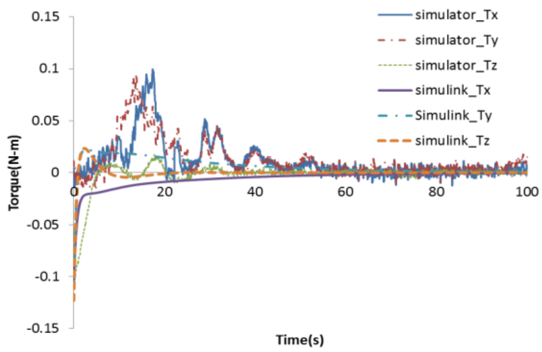

Figure 7. Control effrot in LMI method

By comparing controller efforts obtained from computer and hardware-in-the-loop simulations, it is observed that the spacecraft simulator expresses more control efforts (Figures 6 and 7).

As observed, the reaction wheels work at the end of maneuvers. This remaining level of actuation can be certified by the presence of gravity moment in the experiment situ and air flow disturbance due to manufacturing imprecision in the air-bearing.

In Table 1, a comparison between the two control methods is performed within allowable voltage restrictions in order that motors don't get saturated and controllers can exhibit their best performance.

For the sake of representative comparison, the controllers were tested against standard disturbance terms (sinusoidal, constant and impulse) virtually generated via Labview interface and amplified on the simulator. The maximum value of the modeled disturbance to which the platform responded properly is noticed in Table 2. According to the results, the LMI controller shows more robustness against constant, sinusoidal and impulse disturbances.

TABLE 1. Control Characetics

	Setteling time	Steady-state error	Chattering
LMI simulink	80(s)	0%	-
LMI simulator	150(s)	2%	✓
Robust adaptive simulink	80(s)	0%	-
Robust adaptve simulator	200(s)	2%	-

TABLE 2. Robustness

	Maximum periodic disturbances	Maximum pulse and step disturbances
LMI simulink	$-0.15sin\left(\frac{2\pi t}{400}\right)$	0.015+3.0δ (200,0,2)
LMI simulator	$-0.1sin\left(\frac{2\pi t}{400}\right)$	0.01+2.0δ (200,0,2)
Robust adaptive simulink	$-0.04sin\left(\frac{2\pi t}{400}\right)$	0.004+0.8δ (200,0,2)
Robust adaptve simulator	$-0.01sin\left(\frac{2\pi t}{400}\right)$	0.001+0.2δ (200,0,2)

6. CONCLUSION

The robust control of the 3DoF spacecraft simulator testbed at laboratory setting and computer Simulink details are presented. In the paper, an LMI-based control and a robust adaptive strategy are chosen. The experiments for validating the operation of the designed controllers are described. The results of these experiments confirm the simulator's ability to track and control attitude in 3DoF with these two robust methods under uncertain conditions. The application of the testbed in validating the LMI and robust adaptive control method demonstrates the efficiency of the testbed for the design and testing of GNC methodologies. The experimental results indicate the ability of these robust methods in tracking the desired attitude in a limited time.

7. ACKNOWLEDGMENT

The author would like to thank the Iran National Science Foundation (INSF) (grant number 94003597).

8. REFERENCES

1. Surendran, K., Karthikeyan, K., Kumar, M.D. and Latha, K., "Spacecraft attitude control system simulator", in Process Automation, Control and Computing (PACC), International Conference on, IEEE., (2011), 1-5.
2. Li, Y. and Youhua, G., "Study on attitude control for three degrees of freedom air-bearing spacecraft simulator", in Mechanic Automation and Control Engineering (MACE), International Conference on, IEEE., (2010), 408-411.
3. Wilde, M., Kaplinger, B., Go, T., Gutierrez, H. and Kirk, D., "Orion: A simulation environment for spacecraft formation flight, capture, and orbital robotics", in Aerospace Conference, IEEE., (2016), 1-14.
4. Eun, Y., Park, C. and Park, S.-Y., "Design and development of ground-based 5-dof spacecraft formation flying testbed", in AIAA Modeling and Simulation Technologies Conference., (2016), 1668.
5. Wilde, M., Ciarcià, M., Grompone, A. and Romano, M., "Experimental characterization of inverse dynamics guidance in docking with a rotating target", ***Journal of Guidance, Control, and Dynamics***, (2016), 1173-1187.
6. Xu, Z., Qi, N. and Chen, Y., "Parameter estimation of a three-axis spacecraft simulator using recursive least-squares approach with tracking differentiator and extended kalman filter", ***Acta Astronautica***, Vol. 117, (2015), 254-262.
7. Wu, S., Wang, R., Radice, G. and Wu, Z., "Robust attitude maneuver control of spacecraft with reaction wheel low-speed friction compensation", ***Aerospace Science and Technology***, Vol. 43, (2015), 213-218.
8. Haibin, D., Daobo, W. and Xiufen, Y., "Realization of nonlinear pid with feed-forward controller for 3-dof flight simulator and hardware-in-the-loop simulation", ***Journal of Systems Engineering and Electronics***, Vol. 19, No. 2, (2008), 342-345.
9. Jung, J., Park, S.-Y., Kim, S.-W., Eun, Y. and Chang, Y.-K., "Hardware-in-the-loop simulations of spacecraft attitude synchronization using the state-dependent riccati equation technique", ***Advances in Space Research***, Vol. 51, No. 3, (2013), 434-449.
10. Guarnaccia, L., Bevilacqua, R. and Pastorelli, S.P., "Suboptimal lqr-based spacecraft full motion control: Theory and experimentation", ***Acta Astronautica***, Vol. 122, (2016), 114-136.

11. Simone, C. and Perez, O., "A dynamic, hardware-in-the-loop, three-axis simulator of spacecraft attitude maneuvering with nanosatellite dimensions", ***Journal of Small Satellites***, Vol. 4, No. 1, (2015), 315-322.
12. Malekzadeh, M., Naghash, A. and Talebi, H., "A robust nonlinear control approach for tip position tracking of flexible spacecraft", ***IEEE Transactions on Aerospace and Electronic Systems***, Vol. 47, No. 4, (2011), 2423-2434.
13. Liwei, D., Shenmin, S. and Yong, G., "Attitude control of five degrees of freedom air-bearing platform based on fractional order sliding mode", in Instrumentation, Measurement, Computer, Communication and Control (IMCCC), Third International Conference on, IEEE., (2013), 1530-1534.
14. Mazinan, A., "High-performance robust three-axis finite-time attitude control approach incorporating quaternion based estimation scheme to overactuated spacecraft", ***International Journal of Engineering-Transactions A: Basics***, Vol. 29, No. 1, (2016), 53-60.
15. Zolfaghari, M. and Taher, S., "Fuzzy approximation model-based robust controller design for speed control of bldc motor", ***International Journal of Engineering-Transactions C: Aspects***, Vol. 28, No. 3, (2014), 426-503.
16. Karami-Mollaee, A., "Adaptive fuzzy dynamic sliding mode control of nonlinear systems", ***International Journal of Engineering-Transactions B: Applications***, Vol. 29, No. 8, (2016), 1075-1082.
17. Guglieri, G., Maroglio, F., Pellegrino, P. and Torre, L., "Design and development of guidance navigation and control algorithms for spacecraft rendezvous and docking experimentation", ***Acta Astronautica***, Vol. 94, No. 1, (2014), 395-408.
18. Krstic, M., Kanellakopoulos, I. and Kokotovic, P.V., "Nonlinear and adaptive control design, Wiley, (1995).
19. Sidi, M.J., "Spacecraft dynamics and control: A practical engineering approach, Cambridge university press, Vol. 7, (1997).
20. Wisniewski, R., "Satellite attitude control using only electromagnetic actuation", Citeseer, (1996).

Robust Attitude Control of Spacecraft Simulator with External Disturbances

M. Malekzadeh, B. Shahbazi

Department of Mechanical Engineering, University of Isfahan, Iran

P A P E R I N F O

Paper history:
Received 18 April 2016
Received in revised form 04 January 2017
Accepted 14 February 2017

Keywords:
Spacecraft Attitude Control Simulator
Linear Matrix Inequality
Robust Adaptive Controller
Hardware in the Loop

چکیده

در این مقاله کنترل مقاوم شبیه‌ساز ماهواره، با استفاده از روش نامساوی ماتریسی خطی و روش مقاوم تطبیقی صورت گرفته‌است. شبیه‌ساز ماهواره شامل پلتفرم، یاتاقان هوایی و یک مجموعه سه تایی چرخ عکس العملی است که به عنوان عملگرهای اصلی کنترل وضعیت استفاده می‌شود. سخت افزار شبیه‌ساز، یک حرکت آزاد بلادرنگ سه درجه آزادی فراهم می‌کند. شبیه‌ساز کمک می کند تا یک محیط واقعی برای بررسی عملکرد زیر- سیستم کنترل وضعیت ماهواره به وجود آید. کنترل زاویه ماهواره با استفاده از شبیه‌ساز سه درجه آزادی قابل صحت سنجی است. در این مقاله جزئیاتی راجع به دینامیک اجزا شبیه‌ساز و اغتشاشات وارد به آن ارائه شده است. سپس با توجه به اغتشاشات موجود در محیط و نامعینی-های دینامیکی مدل شده سیستم، دو کنترلر مقاوم نامساوی ماتریسی خطی بر پایه H_∞ و مقاوم تطبیقی در حضور اختلال‌ها و اغتشاش‌ها طراحی شده‌است. نتایج تست، صحت و اعتبار کنترلرهای طراحی شده در کنترل زوایای سمت را نشان می-دهد. نتایج تست‌های آزمایشگاهی توانایی کنترلرهای طراحی شده در شرایط نامعینی ترکیبی (در حضور اغتشاش، عدم قطعیت و نویز حسگرها) را نشان می‌دهد. در این مقاله نتایج شبیه سازی کامپیوتری با تست‌های آزمایشگاهی سخت افزار در حلقه مقایسه شدند.

***doi**: 10.5829/idosi.ije.2017.30.04a.15*